



ELSEVIER

Available online at [www.sciencedirect.com](http://www.sciencedirect.com)

SCIENCE @ DIRECT®

Earth and Planetary Science Letters 225 (2004) 1–17

EPSL

[www.elsevier.com/locate/epsl](http://www.elsevier.com/locate/epsl)

# Basaltic explosive volcanism, but no comet impact, at the Paleocene–Eocene boundary: high-resolution chemical and isotopic records from Egypt, Spain and Denmark

Birger Schmitz<sup>a,\*</sup>, Bernhard Peucker-Ehrenbrink<sup>b</sup>, Claus Heilmann-Clausen<sup>c</sup>,  
Göran Åberg<sup>d</sup>, Frank Asaro<sup>e</sup>, Cin-Ty A. Lee<sup>f</sup>

<sup>a</sup>*Department of Geology, University of Lund, Sölvegatan 12, SE-22362 Lund, Sweden*

<sup>b</sup>*Department of Marine Chemistry and Geochemistry, Woods Hole Oceanographic Institution,  
360 Woods Hole Road, Woods Hole, MA 02543, USA*

<sup>c</sup>*Department of Earth Sciences, Århus University, DK 8000 Århus C, Denmark*

<sup>d</sup>*Institute for Energy Technology, P.O. Box 40, NO-2027 Kjeller, Norway*

<sup>e</sup>*Lawrence Berkeley National Laboratory, University of California, Berkeley, CA 94720, USA*

<sup>f</sup>*Department of Earth Science, Rice University, P.O. Box 1892, Houston, TX 77251, USA*

Received 4 February 2004; received in revised form 14 June 2004; accepted 24 June 2004

Editor: K. Farley

## Abstract

In the search for a triggering mechanism for the Paleocene–Eocene (P–E) boundary event, 55 Ma, centimeter-resolution chemical (e.g., Ir, Os, Pt) and isotope (e.g.,  $^{187}\text{Os}/^{188}\text{Os}$ ,  $^3\text{He}/^4\text{He}$ ,  $^{87}\text{Sr}/^{86}\text{Sr}$ ) records across this boundary have been established for six uplifted marine sections in Egypt, Spain and Denmark. The sections studied represent some of the stratigraphically most complete records across the onset of the carbon isotopic excursion (CIE) and associated benthic foraminifera extinctions that mark the Paleocene–Eocene boundary. High-sensitivity analyses failed to uncover evidence of extraterrestrial element or isotope enrichments in the six sections, refuting the hypothesis of a major comet impact at the boundary. Preliminary searches for other impact-indicative features, such as spherules or shocked quartz, also gave negative results. In the Danish section studied, three basaltic Ir-rich ash layers occur at the Paleocene–Eocene boundary, but no similar ashes were found in Egypt or Spain. The three ashes represent the earliest known manifestation of an unusual 1 to 2 million year long phase of explosive basaltic volcanism in the Færø–Greenland region. This volcanism is synchronous with major flood basalt effusions in East Greenland and is associated with prominent paleogeographic changes in the high-latitude North Atlantic region. Discharge of mantle-derived Os to seawater during this volcanism may explain a small decrease in  $^{187}\text{Os}/^{188}\text{Os}$  ratio at the Paleocene–Eocene boundary in the Zumaya section in Spain.

\* Corresponding author. Tel.: +46 46 2227869; fax: +46 46 2224419.

E-mail address: [birger.schmitz@geol.lu.se](mailto:birger.schmitz@geol.lu.se) (B. Schmitz).

The environmental perturbations at the Paleocene–Eocene boundary appear to have been triggered by basaltic volcanism, but any model for the detailed causal relation remains speculative.

© 2004 Elsevier B.V. All rights reserved.

*Keywords:* Paleocene–Eocene boundary; IETM; comet impact; flood basalt volcanism; iridium; osmium isotopes; carbon isotopic excursion

## 1. Introduction

One of the most dramatic global environmental perturbations during the Cenozoic occurred at the Paleocene–Eocene (P–E) boundary, ca. 55 Ma [1]. The boundary event is characterized by a 2–6‰ negative carbon isotopic excursion (CIE), rapidly escalating global warming, and prominent faunal and floral turnovers (e.g., [1–7]). The CIE developed during less than 10 ky throughout the atmosphere and the entire oceanic water column, requiring that large quantities of isotopically light carbon were added at a high rate to the atmosphere–ocean reservoir [1–4,8]. The resulting greenhouse effect led to the highest temperatures on Earth during at least the Cenozoic [1]. The exceptionally warm conditions lasted for ca. 150 ky during the so-called Initial Eocene Thermal Maximum (IETM) (equivalent to the Paleocene–Eocene Thermal Maximum, see [5]). In connection with the climatic perturbations, deep-sea benthic foraminifera experienced a rapid 35–50% species-loss [2,6]. Planktonic foraminifera diversified into a unique excursion fauna [9], *Apectodinium* dinoflagellates bloomed worldwide in shelf areas [10], and calcareous nannoplankton experienced a significant turnover [11]. On land, archaic mammals were replaced by modern groups such as the odd- and even-toed ungulates and the earliest true primates [7].

Though there is consensus that a CO<sub>2</sub>-induced greenhouse warming occurred at the P–E boundary, the source and mechanism for the rapid addition of large amounts of isotopically light carbon to the ocean–atmosphere carbon reservoir is disputed. The most popular view envisions large-scale decomposition of seafloor methane hydrates and subsequent oxidation of the released CH<sub>4</sub> to CO<sub>2</sub> [8,12]. Carbon in methane hydrates is isotopically fractionated by bacteria towards  $\delta^{13}\text{C}$  values typically as low as –60‰. An alternative hypothesis suggests that the P–E boundary event was triggered by the impact of a 10-km-diameter comet, rich in isotopically light carbon [13]. The comet

contributed about a third of the carbon causing the CIE. Warming due to this initial input of CO<sub>2</sub> triggered seafloor methane hydrate decomposition, which contributed the additional necessary light carbon to create the full CIE. The primary evidence for the comet impact is a small ( $143 \pm 22$  ppt) iridium anomaly at the base of the CIE in the Zumaya section in Spain [14] and the occurrence of magnetic nanophase particles found in kaolinite-rich clay in P–E boundary drill cores in New Jersey. The magnetic nanoparticles were inferred to have formed in an impact-generated vapour cloud [13,15]. Doubts have been raised about an extraterrestrial origin of the Ir anomaly at Zumaya, and the magnetic nanophase particles have been suggested to be of microbial origin [14,16]. Recently, it has been suggested that the P–E boundary CIE formed when voluminous mantle-derived melts penetrated carbon-rich sediments during northeastern Atlantic volcanism. Heating of the sediments mobilized microbial methane to the ocean–atmosphere system through a widespread vent complex dated to the P–E boundary [17].

In order to shed further light on the trigger mechanism for the P–E boundary event, we present detailed platinum group element (PGE), <sup>187</sup>Os/<sup>188</sup>Os, <sup>3</sup>He/<sup>4</sup>He, and <sup>87</sup>Sr/<sup>86</sup>Sr records from six P–E boundary sections generally considered to be stratigraphically expanded and complete. The chemical and isotopic tracers may give indications of the occurrence of extraterrestrial or volcanic minerals or ejecta layers associated with the CIE. The sections represent marine deposits now uplifted and exposed in Egypt, Spain and Denmark (Fig. 1).

## 2. Paleocene–Eocene boundary sections studied

### 2.1. The Dababiya Quarry and Gebel Duwi sections in Egypt

The Global Stratotype Section and Point (GSSP) for the base of the Eocene has recently been defined

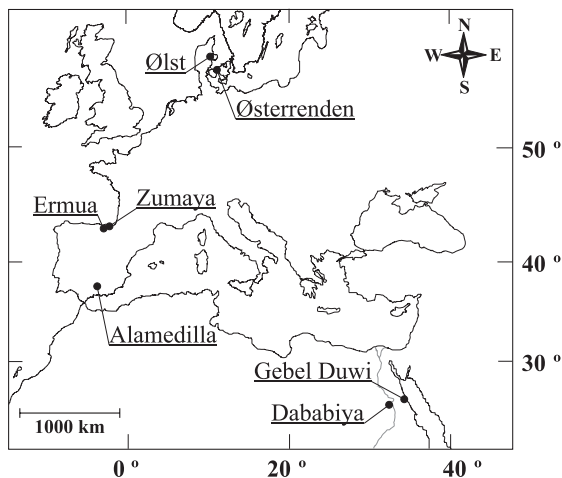


Fig. 1. Map of sites with studied P–E boundary sections.

at the base of the distinct black, anoxic clay that coincides with the base of the CIE in the Dababiya Quarry section in southern Egypt (Fig. 2) [18]. In this section, the rock interval containing the P–E boundary and the CIE occurs in the lower part of an otherwise monotonous ca. 120-m-thick sequence of gray, middle neritic, late Paleocene–early Eocene shales or marls [18]. The carbon isotope records measured on the organic fraction shows an abrupt  $\delta^{13}\text{C}$  decrease from ca.  $-24.4\text{‰}$  to ca.  $-26.0\text{‰}$  over 10-cm vertical distance across the GSSP horizon (Fig. 2). Thereafter,  $\delta^{13}\text{C}$  falls gradually over ca. 1 m upwards to peak excursion values of ca.  $-27.5\text{‰}$ . In total, the CIE extends over 3–4 m of the section. The lower ca. 10 cm of the black clay that marks the basal Eocene is rich in quartz grains of coarse sand size,

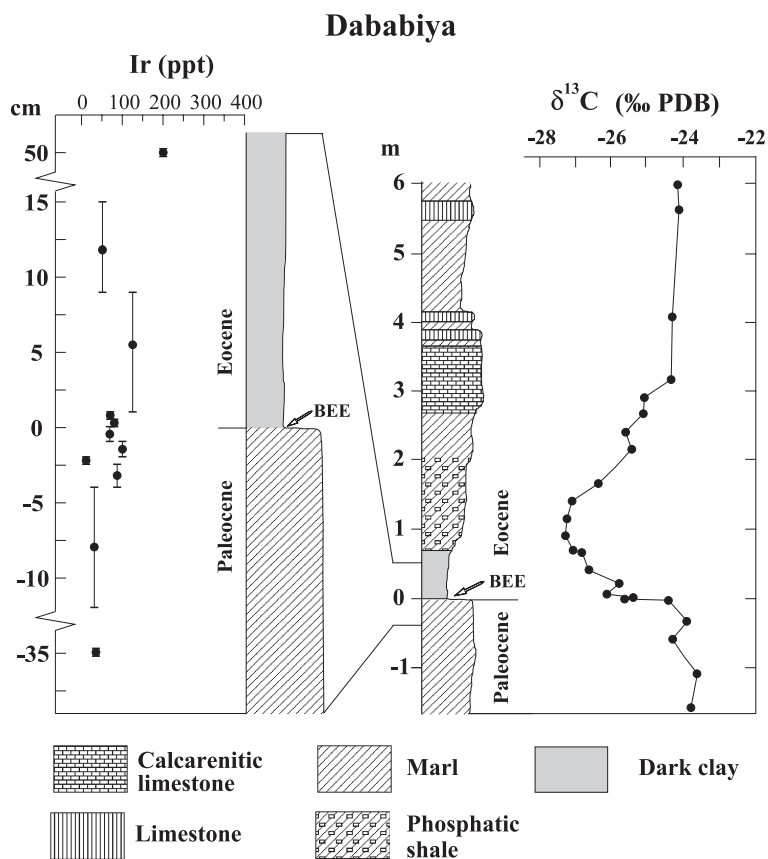


Fig. 2. Iridium results for the P–E boundary section at the Dababiya locality, southern Egypt.



CIE marls and limestone with marl intercalations. Typical Paleocene benthic foraminifera species have their last appearance at the base of the siliciclastic unit [14]. The base of the CIE thus occurs ca. 35 cm below the disappearance of the benthic foraminifera. Schmitz et al. [14] discovered a small iridium anomaly of 143 ppt, over a background of 38 ppt, that coincides with the base of the CIE. The 35-cm separation of the apparent benthic foraminifera extinctions and the base of the CIE may reflect rapid sedimentation and a higher stratigraphic resolution than elsewhere. Very close to or at the onset of the CIE, kaolinite increases abruptly and constitutes 50–75% of the clay fraction throughout the CIE interval [23].

The Ermua section, ca. 25 km SW of Zumaya, formed at the base-of-slope apron, is strongly turbiditic and considerably more expanded across the P–E transition than the Zumaya section, but poorly preserved microfossils and the abundance of turbidites has ruled out its use as global stratotype section (Fig. 4)

[22]. The basic lithological features of the P–E transition at Zumaya, a distinct gray limestone interval, glauconitic at its top, followed by ca. 35 cm of marls underlying a thick siliciclastic unit can be discerned at Ermua as well, but abundant turbidites are dispersed throughout the interval [22]. The siliciclastic unit at Ermua is 20.5 m thick compared to 4 m at Zumaya. At Ermua, the base of the whole-rock CIE has been found, similar to Zumaya, close to the base of the 35 cm (thickness determined excluding turbidites) of marls between the glauconitic limestone and the siliciclastic unit (Fig. 4) [22].

The Alamedilla section is located in the Granada province in southern Spain [24]. This lower bathyal to abyssal section has been recognized as one of the most expanded and continuous across the P–E boundary [11,24–26]. The section contains ca. 30 m of mostly monotonous gray marls spanning calcareous nannoplankton zones NP 9–10 [11]. The CIE is found in the middle part of the section and spans a ca. 3-m-thick red

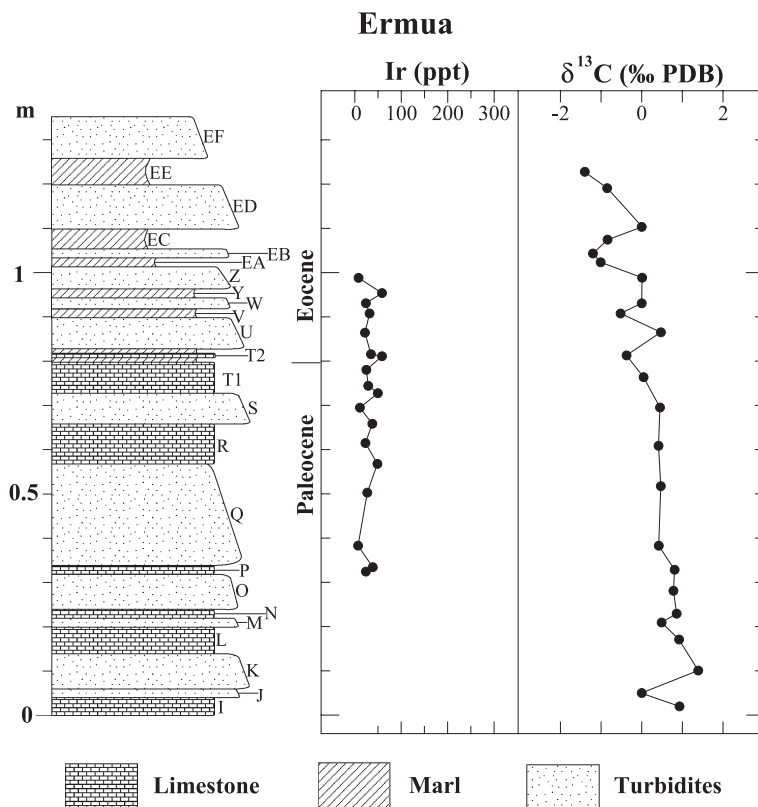


Fig. 4. Iridium results for the P–E boundary section at the Ermua locality, northern Spain.

clay/marl interval, associated with the changes in benthic and planktonic foraminifera and calcareous nannofossils that typify the P–E boundary elsewhere [11,24–26]. The lower ca. 25 cm of this red interval is devoid of calcite. The onset of the CIE coincides with the benthic foraminiferal extinctions occurring at or very close to the base of the 25 cm of red clay [26].

### 2.3. Ølst clay pit section and Østerrenden core in Denmark

In Denmark, the P–E boundary occurs at or very close to the base of the Ølst Formation, which is best studied in the Ølst clay pit in central Jutland, and in the Østerrenden drill core (DGI 83101) from the Store Bælt, southern Denmark. In the Ølst pit section, the CIE is very expanded, spanning the ca. 15 m thick, lower, laminated part of the Ølst Formation (Fig. 5) [27,28]. This part consists of dark gray, noncalcareous clay, rich in organic material and sulfides. *Apectodinium* spp. dinoflagellates, including *Apectodinium augustum*, show a strong acme throughout the interval [29]. Similar *Apectodinium* blooms characterize the IETM interval worldwide [10]. In the Ølst clay pit, the

base of the Ølst Formation is separated by an unconformity from the underlying hemipelagic, bioturbated clays of the Holmehus Formation (of late Thanetian age [30]). In the more continuous record of the Østerrenden core [31], the Ølst Formation is underlain by, in descending order, ca. 3 m of glauconitic silt, ca. 5 m of gray, bioturbated, silty and noncalcareous Østerrende Clay, and the Holmehus Formation. The  $\delta^{13}\text{C}$  record of the organic fraction across this entire interval in the core shows a well-developed CIE beginning at the base of the laminated Ølst Formation and continuing through the laminated interval (Fig. 5) (see [29]). A succession of “numbered” early Eocene ashes, encompassing in ascending order ashes –39 to +140 occurs in Denmark [28,32,33]. The lowermost numbered ashes, –39 to –34, are thin (2 cm and less) and have been found in the laminated part of the Ølst Formation. The lowermost Ølst Formation in the Ølst pit is strongly glauconitic, bioturbated, and grades into laminated clay ca. 15 cm above the unconformity on top of the Holmehus Formation (Fig. 6). In this lithologically continuous interval, representing the crucial transition to an anoxic sea floor, three ash layers occur [28].

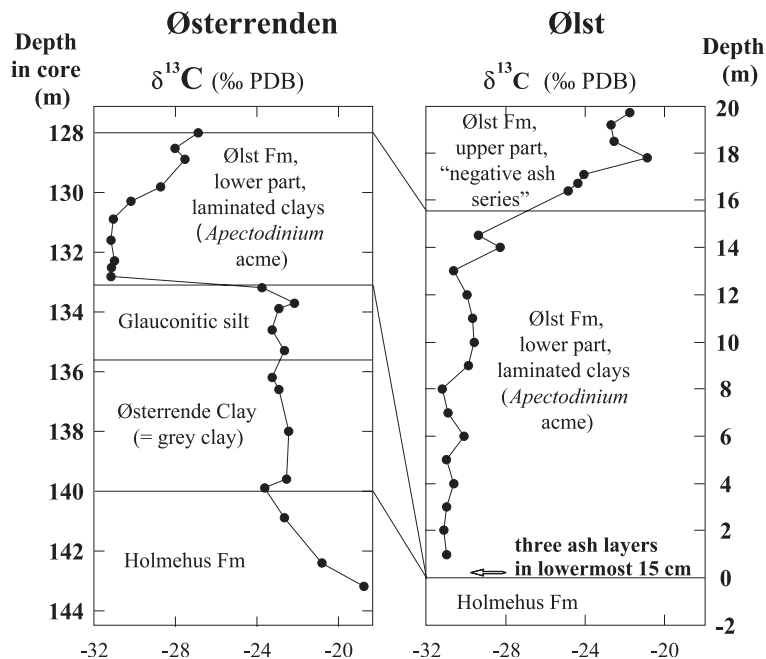


Fig. 5. The P–E boundary sections in the Østerrenden core and in the Ølst clay pit in Denmark.

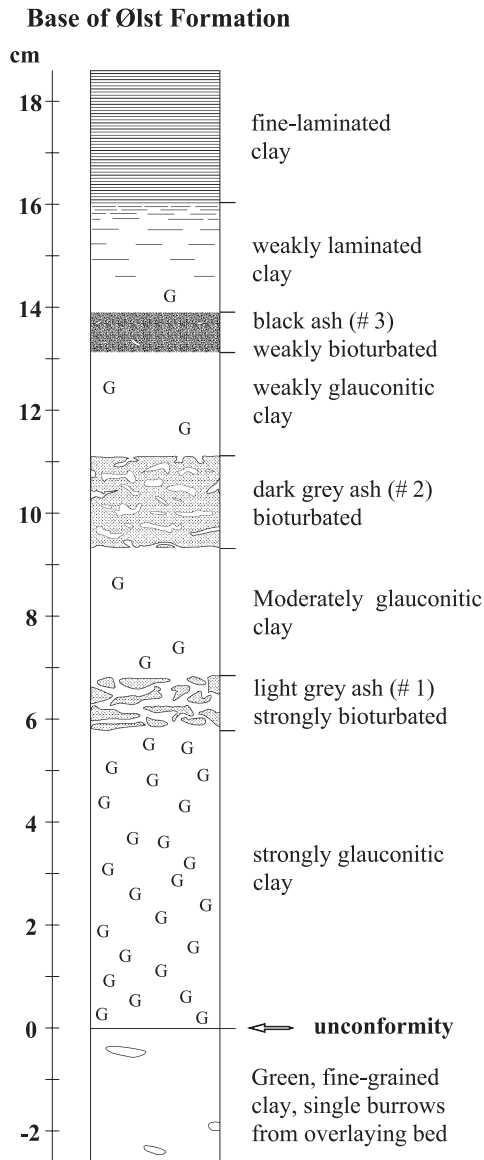


Fig. 6. The basal 18 cm of the Ølst Formation in the Ølst clay pit in Denmark.

These are probably older than the –39 ash and in any case they are from the very beginning of the CIE.

### 3. Samples analyzed

All samples from Egypt and Spain were collected specifically for high-sensitivity PGE analyses, and precautions were taken to avoid contamination.

In the Dababiya Quarry section [18], care was taken to sample the P–E boundary at a spot in the outcrop that was unaffected by sliding and where a continuous P–E boundary transition occurs. A profile with six strip samples each spanning 0.5 to 1.5 cm of the vertical section was collected to cover the entire interval from 4 cm below to 1 cm above the marl–black clay transition (i.e., the formally defined P–E boundary level) (Fig. 2). Five background samples were also collected from 35 cm below to 50 cm above the P–E boundary.

In the Bir Inglisi I section [19,20] at Gebel Duwi, seven strip samples each spanning 0.5 to 1.5 cm of the vertical section were collected to cover the entire interval from 5 cm below to 1 cm above the base of the 1-cm-thick dark shale that marks the P–E boundary. Two background samples from 9–16 and 50 cm below the dark shale were also analyzed.

From the Zumaya section at San Telmo beach [14] samples were collected from a centimeter-thick gray marl interval coinciding with the base of the CIE (Fig. 3). It is in this gray marl that a small Ir anomaly previously has been recorded at Zumaya [14]. From this bed, two fractions were separated for analyses: yellowish marl dispersed throughout the gray bed, and the more common purely gray marl. Samples were also collected at five levels within the overlying 40 cm of greenish marl and from 2 and 1 m below and 0.6 m above the base of the CIE.

From the Ermua section [22], we collected 19 samples spanning representative levels of the transition from gray limestone, glauconitic at its top, to the overlying marls where the base of the CIE is recorded (Fig. 4). The limestone–marl transition corresponds to the interval with an iridium anomaly at nearby Zumaya. Every bed in this interval, including the turbidites, was sampled. From many beds two or more samples were collected in order to cover as much as possible of the stratigraphic interval.

From the Alamedilla section [24], we collected nine strip samples that covered the entire interval from 10 cm below to 9 cm above the transition from calcareous marl to calcite-free red clay associated with the lowermost part of the CIE. One background sample from 25 cm below the marl–red clay transition was also collected.

The three ash layers at the base of the Ølst Formation were sampled in the Ølst clay pit [28] by one of us (CHC) in 1992. The outer exposed and

potentially contaminated areas of the samples were removed with a disposable plastic knife.

#### 4. Chemical and isotopic methods

Sediment aliquots were dried and ground in specially cleaned agate mortars in designated metal-free areas. Os isotope, PGE and Re analyses were performed both at the Woods Hole Oceanographic Institution (WHOI) and at Rice University.

##### 4.1. Os isotope and PGE analyses at WHOI

Samples of sediment powder, 1.8–3.5 g each, were mixed with a PGE tracer solution enriched in  $^{99}\text{Ru}$ ,  $^{105}\text{Pd}$ ,  $^{190}\text{Os}$ ,  $^{191}\text{Ir}$  and  $^{198}\text{Pt}$ , and fused with a flux mixture consisting of borax, nickel and sulfur powders (flux/sample weight ratio of 2) for about 90 min at 1020 °C in a muffle furnace [34]. After separation and dissolution of the NiS bead, insoluble PGE-containing trace particles were filtered onto a 0.45 µm cellulose filter. The filter together with the PGE-rich trace particles were then dissolved in concentrated  $\text{HNO}_3$  at room temperature in sealed Teflon vials. Os concentration and isotopic composition were determined by transferring volatile  $\text{OsO}_4$  from these Teflon vials directly into a single collector magnetic sector ICP-MS (ThermoFinnigan Element 2) [35]. Complementary PGE concentrations were determined on the residual solutions by ICP-MS using a desolvating nebulizer. Analytical blanks as well as precision and accuracy of this method have been investigated in detail [36]. In general,  $^{187}\text{Os}/^{188}\text{Os}$  in homogenous rock standards is reproducible to about 1.5%, whereas PGE concentrations are reproducible to about 6% at the 95% confidence level. Blank-corrected concentrations are reported relative to dry sediment weights.

##### 4.2. Re analyses at WHOI

Sample powder, 50–100 mg, was mixed with a tracer solution enriched in  $^{185}\text{Re}$  and dissolved in a mixture of ultrapure (Seastar) concentrated HF (1 ml), HCl (2 ml) and  $\text{HNO}_3$  (4 ml) in a sealed Teflon vial at ~120 °C overnight. After conversion of the dissolved sample to 0.5 N  $\text{HNO}_3$ , anion exchange chromatography was used to separate Re from the matrix.

Subsequently, Re was analyzed on the single collector magnetic sector ICP-MS (ThermoFinnigan Element 2) using a desolvating nebulizer. Concentrations reported are corrected for analytical blanks (0.35 pg total Re). The standard deviation of the measured  $^{185}\text{Re}/^{187}\text{Re}$  is generally better than 2% for the Zumaya samples and typically better than 0.5% for the Dababiya samples. Reproducibility of Re concentrations is typically better than 5%. Re and Os concentrations were measured on different sample splits.

##### 4.3. Os isotope, PGE and Re analyses at Rice University

Re, Pt, Ir and Os concentrations were determined on the same sample splits by isotope dilution ( $^{185}\text{Re}$ ,  $^{198}\text{Pt}$ ,  $^{191}\text{Ir}$ ,  $^{190}\text{Os}$ ) using a ThermoFinnigan Element 2 ICP-MS. Roughly 1 g of sample powder was combined with a mixed Re, Pt, Ir, and Os spike and reverse aqua regia (~4 g) in a sealed quartz vessel (Carius Tube). The vessel was heated to 230 °C for 72 h. Re, Pt, and Ir were separated using a combination of cation and anion exchange chemistry and analyzed directly by ICP-MS. Os was separated by  $\text{CHCl}_4$  extraction, followed by stabilization as a bromide in HBr solution. This solution was dried down and taken up in 0.1 N HCl for analysis by ICP-MS. For Os isotopic analyses, a separate unspiked aliquot was dissolved. Os was extracted in the same way as above, but it was further purified and concentrated by microdistillation and then analyzed by solution ICP-MS for  $^{187}\text{Os}/^{188}\text{Os}$ ; this final purification step reduced interferences from  $^{187}\text{Re}$  on  $^{187}\text{Os}$  to negligible values. In-run reproducibility ( $2\sigma$ ) for  $^{187}\text{Os}/^{188}\text{Os}$  is <2% for ~100 ppt solution of Os. External reproducibility on comparable standards is <5%. Procedural blanks for Re, Pt, Os and Ir during the course of this study were 4, 10, 3, and 0.6 pg, respectively.

##### 4.4. Iridium coincidence spectrometer analyses

Iridium measurements were performed with the Luis W. Alvarez Iridium Coincidence Spectrometer (LWAICS) at the Lawrence Berkeley National Laboratory [32]. The analytical procedures are described in [32]. Symmetric errors are estimates of the one sigma error in Gaussian statistics and were used when the total number of coincidences exceeded 30. For smaller

numbers of coincidences, estimates from Poisson statistics were used (resulting in asymmetric errors). These errors were adjusted so that the probability that any true abundance, as large as the observed value plus the upper error or as small as the observed value minus the lower error was the same as the one sigma Gaussian probability. These errors converge to the Gaussian values for large numbers of coincidences. Errors with the LWAICS vary with Ir abundances and counting times, so counting times are included in Tables 4, 8 and 9). Scandium concentrations, which can give an indication of variations in clay content, are also included in the tables.

#### 4.5. Helium isotope ratios and concentrations

Powdered samples, 0.5–1.0 g each, were decarbonated with 10% acetic acid (Seastar) at room temperature. This treatment does not affect extraterrestrial He contents in sediments [37]. After completion of the reaction, the slurry was diluted five-fold with ultrapure water (Millipore) and the solution was vacuum-filtered through a 0.45  $\mu\text{m}$ , 47-mm diameter silver membrane filter (Osmonics). This filter size quantitatively captures extraterrestrial He. The filter was washed three times with ultrapure water and reagent-grade isopropanol, left to dry, and folded into a tight package that was wrapped in isopropanol-washed Al-foil to prevent leakage of sediment powder through cracks in the brittle silver membrane filter. The filters were weighted with and without sediment to determine weight loss due to decarbonation. Helium concentrations are reported based on dry bulk sediment weights. Prior to He isotope analysis, the filters were degassed in vacuum for several days to reduce the level of adsorbed volatiles introduced into the noble gas mass spectrometer. Helium isotope analyses were performed in the Isotope Geochemistry Facility at WHOI using a locally constructed noble gas mass spectrometer equipped with a branch-tube, 10 in. radius, 90° magnetic sector and a Nier-type source [38]. Degassed samples were transferred to the resistance furnace operated at 1400 °C equipped with a five-position turret that is connected to a gas mass spectrometer. Interferences can be completely resolved from  $^3\text{He}$ , and  $^3\text{He}$  and  $^4\text{He}$  can be measured simultaneously. Procedural blanks are  $4\text{--}6 \times 10^{-11} \text{ cm}^3 \text{ STP He}$ , and  $^3\text{He}$  detection limits are approximately  $2 \times 10^{-16} \text{ cm}^3 \text{ STP}$  (~5000 atoms).

#### 4.6. Strontium isotope analyses

Strontium isotopes were analyzed at the Institute for Energy Technology, Oslo. Whole-rock samples were leached in HCl (1:1) and rinsed thoroughly in distilled water. About 0.1 g of sediment powder was weighted into Savillex teflon beakers and 3–4 ml concentrated HF and 0.5 ml concentrated  $\text{HNO}_3$  of ultrapure quality were added. The beakers were left on a hot plate at 90 °C overnight. The solution was then evaporated to dryness, 5 ml 6 M HCl of ultrapure quality was added and the solution was heated until the fluorides had been dissolved. Evaporated samples were dissolved in 200  $\mu\text{l}$  ultrapure 3 M  $\text{HNO}_3$ , centrifuged and loaded onto ion-exchange columns packed with an Sr-Spec crown-ether resin from Eichrom, which selectively retained Sr. After rinsing out unwanted elements, Sr was collected with ultrapure water (Millipore). The Sr-fractions were then evaporated to dryness and loaded on pre-gassed Re filaments on a turret holding 12 samples and one NBS 987 Sr standard. Isotopes were determined by thermal ionization mass spectrometry (TIMS) on a Finnigan MAT 261 with a precision of about 20 ppm and an Sr blank of 50–100 pg. The NBS 987 standard gave an  $^{87}\text{Sr}/^{86}\text{Sr}$  ratio of  $0.710231 \pm 0.000015$ .

#### 4.7. Major element analyses

The Danish ashes were analyzed for major elements with an inductively coupled plasma-atomic emission spectrometer (ICP-AES) at Svensk Grundämnesanalys in Luleå, Sweden [32]. Samples were fused with  $\text{LiBO}_2$  and dissolved in  $\text{HNO}_3$ . Samples from the Dababiya and Zumaya sections were fused with  $\text{MoO}_3$ . The fusion pills were polished to a flat surface and analyzed using a LINK Oxford energy dispersive spectrometer with a Ge detector, mounted in a Zeiss DSM 940 scanning electron microscope. A cobalt standard, linked to oxide standards, was used to monitor instrumental drift. The relative reproducibility ( $2\sigma$ ) of the analyses is generally in the range 0.5–6%.

## 5. Results

### 5.1. Egypt

The Ir concentrations across the P–E boundary in the Dababiya section vary between 34 and 128 ppt

(Table 1; Fig. 2), representing typical values for shelf sediments and continental crust [14,39–41]. Only the uppermost sample, 50 cm above the P–E boundary, shows a slightly anomalous Ir value of 200 ppt. A correction for the diluting effect of calcite (ca. 20–30% by weight in the lower part of the profile) does not significantly change this concentration profile (Table 3, see online version of this article). Throughout the studied interval, Os shows significantly elevated concentrations, 960 to 2400 ppt, compared to typical values of 30–50 ppt in continental crustal material [39,41]. The Re concentrations are also strongly elevated throughout the profile, with values in the range 90–290 ppb compared to 0.2–0.4 ppb in average continental crust [39,41]. High Os and Re concentrations reflect hydrogenous scavenging of redox sensitive metals in reducing sediments rich in organic matter (e.g., [42]). Initial  $^{187}\text{Os}/^{188}\text{Os}$  ratios calculated from Re–Os isotope systematics across the P–E boundary at Dababiya give mostly negative results (Table 2), indicating mobility of Re and/or Os after deposition. Seawater during the latest Paleocene–earliest Eocene was characterized by unradiogenic  $^{187}\text{Os}/^{188}\text{Os}$  ranging from 0.32 to 0.44 [43]. The Pd (5.5–12.8 ppb, except for 33 ppb at +50 cm) and Pt (2.4–8.6 ppb) concentrations are similar to values observed in other terrestrial sediments [44]. The PGE concentration ratios throughout the profile are non-chondritic and give no indication for the presence of any significant amounts of extraterrestrial

Table 1  
PGE and Re distributions across the P–E boundary at Dababiya, Egypt<sup>a</sup>

Depth <sup>b</sup> (cm)	Ir (ppt)	Os (ppt)	Pt (ppb)	Pd (ppb)	Re (ppb)
–35	38	960	2.4	6.2	184
–12 to –4	34	1005	2.6	5.7	90
–4 to –2.5	90	1009	3.4	5.8	170
–2.5 to –2.0	14	1066	8.6	5.5	176
–2.0 to –1.0	103	1051	4.2	9.1	181
–1.0 to 0.0	72	1893	5.0	10.5	283
0.0 to 0.5	83	2427	6.3	12.8	286
0.5 to 1.0	73	1802	6.6	10.6	290
1 to 9	128	1410	7.4	11.2	267
9 to 15	54	1115	3.4	10.7	186
50	201	2340	6.3	32.9	208

<sup>a</sup> Analyses at WHOI.

<sup>b</sup> The 0 level is at the base of the black clay, see Fig. 2.

Table 2

Os and Re isotopic distributions across the P–E boundary at Dababiya, Egypt<sup>a</sup>

Depth <sup>b</sup> (cm)	$^{187}\text{Os}/^{188}\text{Os}$ (measured)	$2\sigma_m$	$^{187}\text{Re}/^{188}\text{Os}$	$^{187}\text{Os}/^{188}\text{Os}$ (at 55 Ma) <sup>c</sup>
–35	0.677	0.004	993	–0.23
–12 to –4	0.702	0.005	464	0.28
–4 to –2.5	0.710	0.007	872	–0.09
–2.5 to –2.0	0.692	0.004	855	–0.09
–2.0 to –1.0	0.6882	0.0021	890	–0.13
–1.0 to 0.0	0.662	0.004	772	–0.046
0.0 to 0.5	0.6659	0.0029	608	0.11
0.5 to 1.0	0.6894	0.0023	832	–0.073
1 to 9	0.709	0.004	983	–0.019
9 to 15	0.7770	0.0028	874	–0.024
50	0.841	0.004	469	0.41

<sup>a</sup> Analyses at WHOI.

<sup>b</sup> The 0 level is at the base of the black clay, see Fig. 2.

<sup>c</sup>  $^{187}\text{Re}$  decay constant of  $1.666 \times 10^{-11}$  year<sup>-1</sup> [60].

material. The major element profiles across the P–E boundary do not show evidence for the existence of any distinct ejecta layer nor do they support the presence of substantial amounts of dispersed ejecta material at any level (Table 3, see online version of this article). The  $\text{TiO}_2/\text{Al}_2\text{O}_3$  ratio is a particularly useful proxy for the occurrence of extraneous material in a sedimentary sequence because of the strong resistance of  $\text{TiO}_2$  and  $\text{Al}_2\text{O}_3$  to diagenetic alteration [45]. The  $\text{TiO}_2/\text{Al}_2\text{O}_3$  ratio is stable at a value of 0.04 across the P–E boundary, but increases gradually upwards in the lower part of the black clay, from 0.047 to 0.065. The increase in  $\text{TiO}_2/\text{Al}_2\text{O}_3$  most likely reflects higher depositional hydrodynamic

Table 4  
LWAICS results for P–E boundary at Bir Inglisi I, Egypt

Depth <sup>a</sup> (cm)	Count time (min)	Ir (ppt)	Sc (ppm)
–50	107	9 +28/–9	9.73
–9 to –16	89	0 +14/–0	5.70
–3.5 to –5	94	48 +35/–26	11.92
–2.0 to –3.5	106	17 +30/–17	13.83
–2.0 to –2.5	366	20 +14/–14	12.59
–1.5 to –2.0	116	9 +27/–9	13.83
0 to –1.5	94	12 +33/–12	14.14
0 to 1	147	7 +20/–7	13.34
1 to –1	94	0 +24/–0	13.22

<sup>a</sup> The 0 level is at the base of the 1-cm-thick dark shale just below the fissile pink marls (see [19,20]).

Table 5  
PGE and Re distributions across the P–E boundary at Zumaya, Spain<sup>a</sup>

Depth <sup>b</sup> (m)	Ir (ppt)	Os (ppt)	Pt (ppb)	Pd (ppb)	Re (ppb)
–2.00	37	112	0.65	3.6	0.086
–1.00	37	110	0.52	3.4	0.079
0.00ye	423	192	1.9	11.8	0.21
0.00gr	66	130	1.2	9.6	0.27
0.03	67	170	0.81	9.2	0.48
0.10	78	214	1.5	6.0	0.088
0.27	63	262	1.4	8.9	0.15
0.30	54	205	0.63	3.4	0.088
0.35	50	187	0.73	1.9	0.072
0.60	46	150	0.46	1.6	0.058

ye=yellow fraction; gr=gray fraction.

<sup>a</sup> Analyses at WHOI.

<sup>b</sup> The 0 level is at the base of the greenish marls, see Fig. 3.

energies and an increase in Ti-rich heavy minerals brought to the seafloor together with the coarse quartz that is also present in this interval [45]. The small enrichments of Ir and Pd in the sample 50 cm above the P–E boundary similarly may reflect the occurrence of terrestrial PGE-bearing heavy minerals. No microtektite-shaped objects were found at Dababiya although as much as 2.5 kg of sediment from the boundary interval was sieved (63  $\mu\text{m}$ ) and inspected. Only preliminary searches for shocked quartz were performed, but if shocked quartz grains exist they must be very rare.

The detailed LWAICS results for every centimeter of the P–E boundary transition in the Bir Inglisi I section at Gebel Duwi show that no significant Ir anomaly exists (Table 4).

## 5.2. Spain

The PGE results for the Zumaya section confirm the existence of a small Ir anomaly right at the base of the CIE as previously shown by Schmitz et al. [14] (Table 5; Fig. 3). However, the new data show that the Ir enrichment is confined to the yellowish fraction of the dominantly gray centimeter-thick bed in which the original Ir anomaly of 143 ppt was found. The yellowish fraction contains 423 ppt Ir, compared to 66 ppt Ir in the gray fraction, and ca. 0.5% less  $\text{Fe}_2\text{O}_3$  than the gray fraction (Table 7, see online version of this article). The yellowish fraction likely represents more weathered material in which iron from decomposed glauconite reprecipitated as secondary iron hydroxides that scavenged hydrogenous Ir. Os, Pt and Pd show no significant enrichments in the yellowish fraction (Table 5). The PGE ratios do not give any indication for the presence of a chondritic component in the Ir-rich sample. The results for the remaining part of the P–E profile support the more detailed results of Schmitz et al. [14], showing that there is no other Ir anomaly besides that at the base of the CIE. The other PGEs do not give any indication for the presence of a significant extraterrestrial

Table 6  
Os, Re, Sr and He isotope distributions across the P–E boundary at Zumaya, Spain<sup>a</sup>

Depth <sup>b</sup> (m)	$^{187}\text{Os}/^{188}\text{Os}$ (measured)	$2\sigma_m$	$^{187}\text{Re}/^{188}\text{Os}$	$^{187}\text{Os}/^{188}\text{Os}$ (at 55 Ma) <sup>c</sup>	$^{87}\text{Sr}/^{86}\text{Sr}$	$^3\text{He}$ ( $\text{cm}^3 \text{STP g}^{-1}$ )	$^4\text{He}$ ( $\text{cm}^3 \text{STP g}^{-1}$ )	$^3\text{He}/^4\text{He}$
–2.00	0.464	0.004	3.87	0.461	0.7184	n.a.	n.a.	n.a.
–1.00	0.3892	0.0025	3.54	0.386	0.7200	3.17e–14	2.54e–06	1.25e–08
0.00ye	0.352	0.006	5.51	0.347	0.7223	5.71e–14	1.03e–06	5.54e–08
0.00gr	0.3482	0.0030	10.3	0.339	0.7231	n.a.	n.a.	n.a.
0.03	0.344	0.003	14.0	0.331	0.7221	7.99e–14	1.03e–06	7.75e–08
0.10	0.365	0.005	2.05	0.363	0.7170	n.a.	n.a.	n.a.
0.27	0.3596	0.0023	2.87	0.357	0.7216	n.a.	n.a.	n.a.
0.30	0.3561	0.0024	2.10	0.354	0.7150	n.a.	n.a.	n.a.
0.35	0.380	0.006	1.92	0.379	0.7154	n.a.	n.a.	n.a.
0.60	0.378	0.010	1.92	0.376	0.7140	4.50e–14	1.30e–06	3.46e–08

<sup>a</sup> Os, Re and He isotopic analyses at WHOI; n.a.=not analyzed.

<sup>b</sup> For sample denotations, see Table 5.

<sup>c</sup>  $^{187}\text{Re}$  decay constant of  $1.666 \times 10^{-11} \text{ year}^{-1}$  [60].

Table 8  
LWAICS results for P–E boundary at Ermua, Spain

Bed <sup>a</sup>	Count time (min)	Ir (ppt)	Sc (ppm)
P	3348	23.7±2.7	3.88
Top of P	1111	39±6	7.00
Q-lower	1070	7.2±2.9	1.49
Q-upper	1270	27±4	3.82
Q–R transition	749	49±8	8.26
R	2900	23.4±2.9	3.32
R–S transition	484	38±9	8.29
S	733	10.6±3.6	1.79
S–T transition	1278	50±6	8.21
T1-lower	404	29±8	6.39
Top of T1	1032	25±4	4.22
T2	1328	58±8	14.76
T2 fine fraction	1166	60±8	11.62
T3	290	35±12	9.96
U	895	22±5	3.56
V	1886	32±6	8.54
W	1002	2.4+3.6/–2.4	2.45
Y	1603	59±8	12.91
Z	978	8±4	2.96

<sup>a</sup> For bed denotations, see Fig. 4.

component in the P–E boundary interval at Zumaya (Table 5).

At Zumaya, Re concentrations are low, 0.06–0.48 ppb, and radiogenic ingrowth from <sup>187</sup>Re decay can be neglected. The calculated initial <sup>187</sup>Os/<sup>188</sup>Os ratios, 0.33–0.46, are therefore most likely representative of the initial Os in the section (Table 6). The initial ratios are almost identical to seawater <sup>187</sup>Os/<sup>188</sup>Os ratios at this time, 0.32–0.44 [43]. The <sup>87</sup>Sr/<sup>86</sup>Sr isotopic composition of HCl-leached samples is relatively stable around 0.72 throughout the entire P–E boundary transition (Table 6). These relatively radiogenic Sr isotope values indicate that the major fraction of the siliciclastic fraction at Zumaya represents weathered upper continental crust [46]. Such material typically has Os concentrations around 31 ppt [41] compared to the 110–262 ppt measured at Zumaya. The excess Os is most likely hydrogenous in origin, as supported by the seawater like initial <sup>187</sup>Os/<sup>188</sup>Os ratios. It is noteworthy that the Ir-rich yellowish marl does not differ significantly in <sup>187</sup>Os/<sup>188</sup>Os from adjacent marl with normal Ir concentrations. This similarly argues against an extraterrestrial origin of the excess Ir in the yellowish marl. An important observation is that in the 30-cm-thick interval over which the basal CIE is developed at Zumaya the initial

<sup>187</sup>Os/<sup>188</sup>Os values are slightly less radiogenic (0.33–0.36) than in the four samples from above and below this interval (0.38–0.46). The Sr isotopic and TiO<sub>2</sub>/Al<sub>2</sub>O<sub>3</sub> ratios do not indicate any change in the composition of the siliciclastic fraction over this interval (Table 7, see online version of this article), thus the less radiogenic Os probably reflects a seawater minimum in <sup>187</sup>Os/<sup>188</sup>Os. The <sup>3</sup>He/<sup>4</sup>He ratios in four samples studied are low, 1.3–7.7×10<sup>–8</sup> (Tables 6 and 7), and typical of near-continental marine sediments (e.g., [47] and references therein). The Ir-rich yellowish marl at the base of the CIE is similar in <sup>3</sup>He/<sup>4</sup>He to the background samples. The He isotope data do not provide evidence for a comet impact at the onset of the IETM.

The detailed LWAICS results for the Ermua section near Zumaya and the Alamedilla section in southern Spain show that no significant Ir anomaly is associated with the P–E boundary transition at any of these two sites (Fig. 4; Tables 8 and 9).

### 5.3. Denmark

The three ash layers in the basal Ølst Formation are the same type of basaltic ash layers that are common throughout the rest of the Danish early Eocene [32,33]. This is shown by high TiO<sub>2</sub> concentrations, 2.4–5.3%, and high TiO<sub>2</sub>/Al<sub>2</sub>O<sub>3</sub> ratios, 0.18–0.26 (Table 10, see online version of this article) [32]. The Zr/TiO<sub>2</sub> ratio (ca. 0.005–0.006), another weathering resistant discriminative feature of ashes, and the <sup>87</sup>Sr/<sup>86</sup>Sr ratio (0.705) also suggest that the ashes are

Table 9  
LWAICS results for P–E boundary at Alamedilla, Spain

Depth <sup>a</sup> (cm)	Count time (min)	Ir (ppt)	Sc (ppm)
–25	189	42+21/–17	7.02
–10 to –7.5	81	20+32/–20	6.87
–7.5 to –5	76	23+36/–24	7.72
–5 to –3	79	47+38/–27	7.82
–3 to –1	82	43+37/–27	8.53
0 to –1(gray)	116	50+31/–24	8.32
0 to 1	91	29+45/–34	16.23
0 to 3	93	18+40/–18	15.94
3 to 6	314	60+20/–20	15.52
6 to 9	398	40+17/–17	15.19

<sup>a</sup> The 0 level is at the base of the P–E boundary red clay.

basaltic. Just like other Danish early Eocene basaltic ashes, the three at the base of the Ølst Formation are rich in Ir (220–310 ppt) and Os (460–610 ppt). The  $^{187}\text{Os}/^{188}\text{Os}$  ratios of the ashes (0.33–0.50), however, are surprisingly similar to ratios estimated for latest Paleocene–earliest Eocene seawater (0.32–0.44), rather than to mantle material (ca. 0.13) [48]. Because the Re concentrations are low (8–20 ppb), initial  $^{187}\text{Os}/^{188}\text{Os}$  ratios do not differ much from measured ratios. The three ashes in the basal Ølst Formation are strongly diagenetically altered and lack glass unlike the glass-rich “positive” ashes of the Fur Formation. This explains some differences in major element chemistry, e.g., for MgO, CaO, Fe<sub>2</sub>O<sub>3</sub> (Table 10).

## 6. Discussion

### 6.1. Major comet impact at the P–E boundary?

The suggestion by Kent et al. [13,15] that a major comet impact triggered the P–E boundary event is based primarily on three pieces of evidence: (1) the occurrence of unusual remanent magnetization in the IETM interval in drill cores from the Atlantic Coastal Plain of New Jersey, (2) the previously reported small Ir anomaly at the P–E boundary at Zumaya [14], and (3) the CIE itself. According to the hypothesis of Kent et al., the light carbon that was added to the carbon reservoir at the onset of the CIE derived from the comet itself. Unless the comet was unusually dust-poor, one would expect that extraterrestrial PGE-rich detritus was dispersed in the environment together with the comet-derived carbon, creating at least weak PGE anomalies in the geological record. The results from this study lend no support for the occurrence of significant PGE anomalies of extraterrestrial origin in any section. The small iridium anomaly associated with the base of the CIE at Zumaya is not of extraterrestrial origin. This is clearly shown by a lack of a corresponding significant negative  $^{187}\text{Os}/^{188}\text{Os}$  anomaly, an overall terrestrial PGE pattern and absence of a  $^3\text{He}/^4\text{He}$  anomaly in the Ir-rich sample. The Ir anomaly from Zumaya could neither be reproduced in the more expanded, nearby section at Ermua nor in any of the other four sections studied. The small decline in  $^{187}\text{Os}/^{188}\text{Os}$ , from 0.38–0.46 to 0.33–0.36 across the 30-cm interval that records the

onset of the CIE at Zumaya could, as one of several possibilities, reflect the admixture of a minute excess amount of extraterrestrial matter. However, this excess amount would represent less than ca. 20% of the total Os content of the samples, and would correspond to an Os anomaly of ca. 30 ppt, as compared to ca. 400,000 ppt in chondritic meteorites. Such a small enrichment could possibly be related to a minor comet or asteroid impact, but does not represent support for the impact scenario of Kent et al. A more likely explanation is that the drop in  $^{187}\text{Os}/^{188}\text{Os}$  is linked to basaltic volcanism in the North Atlantic region (see next section).

A further observation in this study is that in the Spanish and Egyptian sections there is no evidence for any lithologically discernible ejecta layer, volcanic or impact-related, associated with the P–E boundary. Neither is there evidence for the admixture of significant amounts of extraneous material with an origin other than typical continental crust or terrestrial sediments. The Sr isotope and TiO<sub>2</sub>/Al<sub>2</sub>O<sub>3</sub> ratios of clay are sensitive to admixture of even small amounts of basaltic detritus, but these proxies show no significant variations across the P–E boundary at Zumaya. Admixture of 5% of basaltic detritus like that found at the P–E boundary in Denmark with the background clay at Zumaya would result in a shift in TiO<sub>2</sub>/Al<sub>2</sub>O<sub>3</sub> ratio from 0.04 to 0.05, a shift clearly not seen (Table 7).

There are several other arguments against the comet impact scenario of Kent et al. These authors propose that the pure, very fine-grained kaolinites that come in at the base of the CIE in the Atlantic Coastal Plain cores represent reworked impact ejecta debris [13]. The same type of very fine-grained kaolinites dominates the clay fraction, for example, also over several meters associated with the CIE at Zumaya. The stratigraphic interval rich in kaolinite at Zumaya does not show any Ir enrichments (Fig. 3) or anomalous Sr-isotope or TiO<sub>2</sub> concentrations, which would be the case in most situations if the kaolinites represent extraneous impact ejecta. The fact that the kaolinite-dominated CIE beds are several meters thick (and fine-grained) both in Spain and New Jersey also argues against an ejecta origin. A several meter thick impact ejecta layer at both sides of the Atlantic would require ejection of unrealistically large amounts of target rock. For comparison, the Cretaceous–Tertiary

boundary impact ejecta layer is ca. 1–2 cm thick over North America and only some millimeters thick in Europe. The kaolinite enrichment at Zumaya has instead been shown to be related to a sea-level fall and change in weathering regime during the greenhouse conditions at the IETM [5]. A very detailed He isotopic study across one of the most complete deep-sea drilling P–E boundary sections, ODP Hole 690B at Maud Rise in the Southern Ocean, shows a decline in extraterrestrial  $^3\text{He}$  at the P–E boundary [47]. A comet impacting Earth would most likely have been accompanied by significant amounts of  $^3\text{He}$ -rich dust that would have settled on Earth in connection with the impact.

### 6.2. A volcanic trigger of the P–E boundary event?

The global changes at the P–E boundary have repeatedly been proposed to be somehow related to the basaltic volcanism associated with the opening of the Greenland-Norwegian sea [49–52]. The stratigraphic coincidence of the three earliest basaltic ashes from this volcanism with the base of the CIE in the Ølst section in Denmark provides support for a volcanic trigger mechanism. Previous discussions on the role of volcanism have suffered from a lack of understanding (see, in particular, [51,53]) of the temporal relations between different events, but with the CIE and its great correlation potential, the picture is becoming clearer.

Knox [50,52] has shown that Paleocene–early Eocene volcanism in the North Sea/Færø-Greenland region is confined to two phases, with phase 1 occurring in the mid-Paleocene and phase 2 starting at about the P–E boundary and continuing for ca. 1.5 to 2 My. The second phase is divided into subphases 2.1, 2.2a and 2.2b, with 2.1 corresponding approximately to the lower part of the negative ash series in Denmark, phase 2.2a to the upper negative ashes, and 2.2b to the positive ash layers. Phase 2.2b is the major phase of basaltic ash ejection represented by 140 positively numbered ashes in the Fur Formation, ashes that can be traced to Austria and the Bay of Biscay [32,33,54]. These ashes are predominantly tholeiitic basaltic and represent the most significant phase of seafloor spreading between Greenland and Norway [32,33]. This phase of volcanism, however, clearly postdates the environmental perturbations at the P–E

boundary. The negative series of ashes, –1 to –39, in Denmark, represents a more mixed assemblage of rhyolitic, mafic alkaline and basaltic ashes and are commonly inferred to represent continental rifting and embryonic seafloor spreading [32,33]. Phase 2.1 corresponds in time approximately to the IETM interval and possibly also some time just after the IETM. From phase 2.1 only about 20 ash layers are known and they are almost all thin (<2 cm). The three basaltic ashes at the base of the CIE in the Ølst section represent the earliest ashes of phase 2.1.

Larsen et al. [33] pointed out that the extremely high magma production that led to the huge subaerial flood basalts in East Greenland probably preceded the formation of the North Sea positive ash series. Therefore, the positive ashes do not mark a peak of magmatic activity, but rather mark a switch from effusive to explosive volcanism. A similar conclusion was reached by Waagstein and Heilmann-Clausen [55], who showed that proximal basaltic tuffs overlie the plateau basalts on the Færøes shelf. It is therefore most likely that the earliest negatively numbered ash layers (–39 to –22) coincide with major effusive volcanism along the East Greenland and Færøes shelves. The earliest ash layers of phase 2.1 in previously studied stratigraphically complete sections (the Viborg-1 and Østerrende boreholes [31,56]), as well as the three basaltic ash layers reported here, were all deposited at the beginning of the acme of *Apectodinium* spp. (with *A. augustum*) in the basal part of the Ølst Formation, during the onset of the CIE. Our results thus indicate synchronicity between the onsets of the CIE and basaltic ash ejection of phase 2.1 with major effusive magmatic activity in the Færø-Greenland region [57]. The small decrease in  $^{187}\text{Os}/^{188}\text{Os}$  in the sediments at the P–E boundary in Zumaya may also be the signature of a major phase of basaltic lava effusion.

Although the temporal coincidence of the CIE with the onset of basaltic volcanism favors a volcanic triggering mechanism, the origin of the isotopically light  $\text{CO}_2$  that created the CIE remains speculative. Dickens et al. [8] argue that magmatic  $\text{CO}_2$  is not a likely source. As magmatic  $\text{CO}_2$  has  $\delta^{13}\text{C}$  of about –6‰ it would require unrealistically large amounts of this type of carbon to create the observed CIE. Recently, it has been proposed that the CIE formed when mantle-derived melts in carbon-rich sedimentary strata of the Norwegian Sea mobilized large

quantities of microbial methane to the ocean–atmosphere system [17]. This is supported by a vast hydrothermal vent complex that appears to have formed at the floor of the Norwegian Sea at the start of the IETM interval. We suggest as an alternative scenario that magmatic activity triggered paleogeographic change that led to greenhouse climate. There is evidence along the North Atlantic margins of a rapid, dramatic sea-level fall occurring contemporaneously with the P–E boundary event [5,28,50,52]. Large shelf and epicontinental sea areas along the North Atlantic margins and particularly in the northern high latitudes became exposed above sea level. Microbially mediated methane in the pores of the uplifted shelf sediments invaded the atmosphere. Remaining submerged areas, including perhaps the basin that evolved into the present Arctic Ocean, experienced shallower depths. Reduced hydrostatic pressures at the seafloor triggered decomposition of methane hydrates in the sediments, further adding light carbon to the atmosphere.

Bralower et al. [58] related the IETM to late Paleocene–early Eocene circum-Caribbean explosive, non-mafic volcanism; however, such volcanism has been common throughout most of Earth’s history. Non-mafic explosive volcanism has probably been ongoing somewhere on Earth during all times and any global event in the past coincides in time with such volcanism in some regions. Major flood basalt eruptions are more rare, there is a discussion whether they are responsible for some of the major mass extinction events [59].

## 7. Conclusions

Detailed PGE and isotope analyses of six continuous sections across the P–E boundary show that this event was not triggered by the impact of an extraterrestrial body. The finding that the onset of basaltic ash ejection in the North Sea region coincides with the P–E boundary instead suggests a volcanic trigger. The volcanic ashes are related to the major episode of flood basalt eruption in connection with the earliest stages of the opening of the Norwegian–Greenland Sea. The volcanism led indirectly to seafloor methane release, triggering greenhouse conditions in the earliest Eocene.

## Acknowledgements

We are grateful to E. Molina, K. Ouda with colleagues and V. Pujalte for help with collection of samples and to A. Cronholm for assistance throughout. We thank L. Ball and D. Schneider of the WHOI-ICP Facility for the use of their ThermoFinnigan Element 2 and T. Abbruzzese for preparing samples for analyses. The He isotope analyses were performed in the WHOI Isotope Geochemistry Facility supervised by W.J. Jenkins, M.D. Kurz, D. Lott and J. Curtice. We are particularly indebted to M.D. Kurz and J. Curtice for making the He isotope measurements. This is WHOI contribution number 11159. We thank the Department of Earth Science at Rice University for support in developing laboratory facilities. Reviews by T.J. Bralower and F.T. Kyte improved the manuscript considerably. The project was funded by the Swedish Research Council and the US National Science Foundation.

## Appendix A. Supplementary Data

Supplementary data associated with this article can be found, in the online version, at [doi:10.1016/j.epsl.2004.06.017](https://doi.org/10.1016/j.epsl.2004.06.017).

## References

- [1] J. Zachos, M. Pagani, L. Sloan, E. Thomas, K. Billups, Trends, rhythms, and aberrations in global climate 65 Ma to present, *Science* 292 (2001) 686–693.
- [2] J.P. Kennett, L.D. Stott, Abrupt deep-sea warming, palaeoceanographic changes and benthic extinctions at the end of the Palaeocene, *Nature* 353 (1991) 225–229.
- [3] S. Bains, R.M. Corfield, R.D. Norris, Mechanisms of climate warming at the end of the Paleocene, *Science* 285 (1999) 724–727.
- [4] D.J. Thomas, J.C. Zachos, T.J. Bralower, E. Thomas, S. Bohaty, Warming the fuel for the fire: evidence for the thermal dissociation of methane hydrate during the Paleocene–Eocene thermal maximum, *Geology* 30 (2002) 1067–1070.
- [5] B. Schmitz, V. Pujalte, Sea-level, humidity, and land-erosion records across the initial Eocene thermal maximum from a continental-marine transect in northern Spain, *Geology* 31 (2003) 689–692.
- [6] E. Thomas, Biogeography of the late Paleocene benthic foraminiferal extinction, in: M.-P. Aubry, S. Lucas, W.A.

- Berggren (Eds.), Late Paleocene–Early Eocene Climatic and Biotic Events in the Marine and Terrestrial Records, Columbia University Press, New York, 1998, pp. 214–243.
- [7] P.D. Gingerich, Mammalian responses to climate change at the Paleocene–Eocene boundary: Polecat Bench record in the northern Bighorn Basin, Wyoming, in: S.L. Wing, P.D. Gingerich, B. Schmitz, E. Thomas (Eds.), Causes and Consequences of Globally Warm Climates in the Early Paleogene, Geological Society of America Special Paper, 369, 2003, pp. 463–478.
- [8] G.R. Dickens, J.R. O’Neil, D.K. Rea, R.M. Owen, Dissociation of oceanic methane hydrate as a cause of the carbon isotope excursion at the end of the Paleocene, *Paleoceanography* 10 (1995) 965–971.
- [9] D.C. Kelly, T.J. Bralower, J.C. Zachos, I. Premoli Silva, E. Thomas, Rapid diversification of planktonic foraminifera in the tropical Pacific (ODP Site 865) during the late Paleocene thermal maximum, *Geology* 24 (1996) 423–426.
- [10] E.M. Crouch, C. Heilmann-Clausen, H. Brinkhuis, H.E.G. Morgans, K.M. Rogers, H. Egger, B. Schmitz, Global dinoflagellate event associated with the late Paleocene thermal maximum, *Geology* 29 (2001) 315–318.
- [11] S. Monechi, E. Angori, K. von Salis, Calcareous nannofossil turnover around the Paleocene/Eocene transition at Alamedilla (southern Spain), *Bulletin de la Société Géologique de France* 171 (2000) 477–489.
- [12] G.R. Dickens, Rethinking the global carbon cycle with a large, dynamic and microbially mediated gas hydrate capacitor, *Earth and Planetary Science Letters* 213 (2003) 169–183.
- [13] D.V. Kent, B.S. Cramer, L. Lanci, D. Wang, J.D. Wright, R. Van der Voo, A case for a comet impact trigger for the Paleocene/Eocene thermal maximum and carbon isotope excursion, *Earth and Planetary Science Letters* 211 (2003) 13–26.
- [14] B. Schmitz, F. Asaro, E. Molina, S. Monechi, K. von Salis, R.P. Speijer, High-resolution iridium,  $\delta^{13}\text{C}$ ,  $\delta^{18}\text{O}$ , foraminifera and nannofossil profiles across the latest Paleocene benthic extinction event at Zumaya, Spain, *Palaeogeography, Palaeoclimatology, Palaeoecology* 133 (1997) 49–68.
- [15] D.V. Kent, B.S. Cramer, L. Lanci, D. Wang, J.D. Wright, R. Van der Voo, Reply to a comment on “A case for a comet impact trigger for the Paleocene/Eocene thermal maximum and carbon isotope excursion” by G.R. Dickens and J.M. Francis, *Earth and Planetary Science Letters* 217 (2003) 201–205.
- [16] G.R. Dickens, J.M. Francis, Comment on “A case for a comet impact trigger for the Paleocene/Eocene thermal maximum and carbon isotope excursion” by D.V. Kent et al., *Earth and Planetary Science Letters* 217 (2003) 197–200.
- [17] H. Svensen, S. Planke, A. Malthe-Sørenssen, B. Jamtveit, R. Myklebust, T. Rasmussen Eidem, S.S. Rey, Release of methane from a volcanic basin as a mechanism for initial Eocene global warming, *Nature* 429 (2004) 542–545.
- [18] C. Dupuis, M.P. Aubry, E. Steurbaut, W.A. Berggren, K. Ouda, R. Magioncalda, B.S. Cramer, D.V. Kent, R.P. Speijer, C. Heilmann-Clausen, The Dababiya Quarry section: lithostratigraphy, clay mineralogy, geochemistry and paleontology, *Micropaleontology* 49 (2003) 41–59.
- [19] R.P. Speijer, B. Schmitz, P. Luger, Stratigraphy of late Paleocene events in the Middle East: implications for low- to middle-latitude successions and correlations, *Geological Society of London Journal* 157 (2000) 37–47.
- [20] R.P. Speijer, G.J. van der Zwaan, B. Schmitz, The impact of Paleocene/Eocene boundary events on middle neritic benthic foraminiferal assemblages from Egypt, *Marine Micropaleontology* 28 (1996) 99–132.
- [21] J. Dinarès-Turell, J.I. Baceta, V. Pujalte, X. Orue-Etxebarria, G. Bernaola, Magnetostratigraphic and cyclostratigraphic calibration of a prospective Paleocene/Eocene stratotype at Zumaia (Basque Basin, northern Spain), *Terra Nova* 14 (2002) 371–378.
- [22] B. Schmitz, V. Pujalte, K. Nunez-Betelu, Climate and sea-level perturbations during the initial Eocene thermal maximum: evidence from siliciclastic units in the Basque Basin (Ermua, Zumaia and Trabakua Pass), northern Spain, *Palaeogeography, Palaeoclimatology, Palaeoecology* 165 (2001) 299–320.
- [23] R.W. O’B. Knox, Kaolinite influx within Paleocene/Eocene boundary strata of western Europe, *Newsletters on Stratigraphy* 36 (1998) 49–53.
- [24] I. Arenillas, E. Molina, Biostratigrafía y evolución de las asociaciones de foraminíferos planctónicos del tránsito Paleoceno–Eoceno en Alamedilla (Cordilleras Béticas), *Revista Española de Micropaleontología* 28 (1996) 75–96.
- [25] E. Molina, I. Arenillas, A. Pardo, High resolution planktonic foraminiferal biostratigraphy and correlation across the Paleocene/Eocene boundary in the Tethys, *Bulletin de la Société Géologique de France* 170 (1999) 521–530.
- [26] G. Lu, G. Keller, T. Adatte, N. Ortiz, E. Molina, Long-term ( $10^5$ ) or short-term ( $10^3$ )  $\delta^{13}\text{C}$  excursion near the Paleocene–Eocene transition: evidence from the Tethys, *Terra Nova* 8 (1996) 347–355.
- [27] C. Heilmann-Clausen, O.B. Nielsen, F. Gersner, Lithostratigraphy and depositional environments in the Upper Paleocene and Eocene of Denmark, *Bulletin of the Geological Society of Denmark* 33 (1985) 287–323.
- [28] C. Heilmann-Clausen, *Palaeogene aflejringer over Danskekalken*, Aarhus Geokompender, vol. 1, Geological Institute, Aarhus University, 1995, pp. 69–114.
- [29] C. Heilmann-Clausen, B. Schmitz, The late Paleocene thermal maximum  $\delta^{13}\text{C}$  excursion in Denmark? *GFF* 122 (2000) 70.
- [30] C. Beyer, C. Heilmann-Clausen, N. Abrahamsen, Magnetostratigraphy of the Upper Paleocene–lower Eocene deposits in Denmark, *Newsletters on Stratigraphy* 39 (2001) 1–19.
- [31] O.B. Nielsen, C. Heilmann-Clausen, Lithology of the Tertiary section, in: J.T. Møller (Ed.), Twenty five years of geology in Aarhus, vol. 25, Aarhus Universitet, Geoskrifter, 1986, pp. 235–253.
- [32] B. Schmitz, F. Asaro, Iridium geochemistry of volcanic ash layers from the early Eocene rifting of the northeastern North Atlantic and some other Phanerozoic events, *Geological Society of America Bulletin* 108 (1996) 489–504.

- [33] L.M. Larsen, J.G. Fitton, A.K. Pedersen, Paleogene volcanic ash layers in the Danish Basin: compositions and source areas in the North Atlantic Igneous Province, *Lithos* 71 (2003) 47–80.
- [34] G. Ravizza, D. Pyle, PGE and Os isotopic analyses of single sample aliquots with NiS fire assay preconcentration, *Chemical Geology* 141 (1997) 251–268.
- [35] D.R. Hassler, B. Peucker-Ehrenbrink, G.E. Ravizza, Rapid determination of Os isotopic compositions by sparging OsO<sub>4</sub> into a magnetic-sector ICP-MS, *Chemical Geology* 166 (2000) 1–14.
- [36] B. Peucker-Ehrenbrink, W. Bach, S.R. Hart, J.S. Blusztajn, T. Abbruzzese, Rhenium–osmium isotope systematics and platinum group element concentrations in oceanic crust from DSDP/ODP Sites 504 and 417/418, *Geochemistry, Geophysics, Geosystems* 4 (2003) DOI:10.1029/2002GC000414.
- [37] D.B. Patterson, K.A. Farley, Extraterrestrial <sup>3</sup>He in seafloor sediments: evidence for correlated 100 kyr periodicity in the accretion rate of interplanetary dust, orbital parameters, and Quaternary climate, *Geochimica et Cosmochimica Acta* 62 (1998) 3669–3682.
- [38] M.D. Kurz, J.J. Gurney, W.J. Jenkins, D.E. Lott III, Helium isotopic variability within single diamonds from the Orapa kimberlite pipe, *Earth and Planetary Science Letters* 86 (1987) 57–68.
- [39] K.H. Wedepohl, The composition of the continental crust, *Geochimica et Cosmochimica Acta* 59 (1995) 1217–1232.
- [40] F.D. Fenner, B.J. Presley, Iridium in Mississippi River suspended matter and Gulf of Mexico sediment, *Nature* 312 (1984) 260–262.
- [41] B. Peucker-Ehrenbrink, B.M. Jahn, Rhenium–osmium isotope systematics and platinum group element concentrations: loess and the upper continental crust, *Geochemistry, Geophysics, Geosystems* 2 (2001) DOI:10.1029/2001GC000172.
- [42] B. Peucker-Ehrenbrink, G. Ravizza, The marine osmium isotope record, *Terra Nova* 12 (2000) 205–219.
- [43] G. Ravizza, R.N. Norris, J. Blusztajn, M.-P. Aubry, An osmium isotope excursion associated with the late Paleocene thermal maximum: evidence of intensified chemical weathering, *Paleoceanography* 16 (2001) 155–163.
- [44] N.J. Evans, D.C. Gregoire, W.D. Goodfellow, B.I. McInnes, N. Miles, J. Veizer, Ru/Ir ratios at the Cretaceous–Tertiary boundary: implications for PGE source and fractionation within the ejecta cloud, *Geochimica et Cosmochimica Acta* 57 (1993) 3149–3158.
- [45] B. Schmitz, The TiO<sub>2</sub>/Al<sub>2</sub>O<sub>3</sub> ratio in the Cenozoic Bengal abyssal fan sediments and its use as a paleostream energy indicator, *Marine Geology* 76 (1987) 195–206.
- [46] B. Schmitz, S.I. Ingram, D.T. Dockery III, G. Åberg, Testing <sup>87</sup>Sr/<sup>86</sup>Sr as a paleosalinity indicator on mixed marine, brackish-water and terrestrial vertebrate skeletal apatite in late Paleocene–early Eocene near-coastal sediments, Mississippi, *Chemical Geology* 140 (1997) 275–287.
- [47] K.A. Farley, S.F. Eltgroth, An alternative age model for the Paleocene–Eocene thermal maximum using extraterrestrial <sup>3</sup>He, *Earth and Planetary Science Letters* 208 (2003) 135–148.
- [48] T. Meisel, R.J. Walker, J.W. Morgan, The osmium isotopic composition of the Earth's primitive upper mantle, *Nature* 383 (1996) 517–520.
- [49] O. Eldholm, E. Thomas, Environmental impact of volcanic margin formation, *Earth and Planetary Science Letters* 117 (1993) 319–329.
- [50] R.W. O'B. Knox, The tectonic and volcanic history of the North Atlantic Region during the Paleocene–Eocene transition: implications for NW European and Global biotic events, in: M.-P. Aubry, S. Lucas, W.A. Berggren (Eds.), *Late Paleocene–Early Eocene Climatic and Biotic Events in the Marine and Terrestrial Records*, Columbia University Press, New York, 1998, pp. 91–102.
- [51] D.W. Jolley, B. Clarke, S. Kelley, Paleogene time scale miscalibration: evidence from the dating of the North Atlantic igneous province, *Geology* 30 (2002) 7–10.
- [52] R.W.O'B. Knox, Tectonic controls on sequence development in the Palaeocene and earliest Eocene of southeast England: implications for North Sea stratigraphy, in: S.P. Hesselbo, D.N. Parkinson (Eds.), *Sequence Stratigraphy in British Geology*, Geological Society Special Publication, vol. 103, 1996, pp. 209–230.
- [53] Paleogene time scale miscalibration: evidence from the dating of the North Atlantic igneous province: comments and replies, *Geology* 31 (2003) 467–472.
- [54] H. Egger, C. Heilmann-Clausen, B. Schmitz, The Paleocene–Eocene boundary interval of a Tethyan deep-sea section and its correlation with the North Sea Basin, *Bulletin de la Société Géologique de France* 171 (2000) 207–216.
- [55] R. Waagstein, C. Heilmann-Clausen, Petrography and biostratigraphy of Palaeogene volcanoclastic sediments dredged from the Færøes shelf, in: R.A. Scrutton, et al., (Eds.), *The Tectonics, Sedimentation and Paleooceanography of the North Atlantic Region*, Geological Society, London, Special Publication, 90, 1995, pp. 179–198.
- [56] C. Heilmann-Clausen, Dinoflagellate stratigraphy of the uppermost Danian to Ypresian in the Viborg 1 borehole, central Jylland, Denmark, *Danmarks Geologiske Undersøgelse. Serie A* 7 (1985) 1–69.
- [57] D.W. Jolley, B.R. Bell, The evolution of the North Atlantic Igneous Province and the opening of the NE Atlantic rift, in: D.W. Jolley, B.R. Bell (Eds.), *The North Atlantic Igneous Province: Stratigraphy, Tectonic, Volcanic and Magmatic Processes*, Geological Society, London, Special Publications, vol. 197, 2002, pp. 1–13.
- [58] T.J. Bralower, D.J. Thomas, J.C. Zachos, M.M. Hirschmann, U. Röhl, H. Sigurdsson, E. Thomas, D.L. Whitney, High-resolution records of the late Paleocene thermal maximum and circum-Caribbean volcanism: Is there a causal link? *Geology* 25 (1997) 963–966.
- [59] W. Alvarez, Comparing the evidence relevant to impact and flood basalt at times of major mass extinctions, *Astrobiology* 3 (2003) 153–161.
- [60] M.I. Smoliar, R.J. Walker, J.W. Morgan, Re–Os ages of group IIA, IIIA, IVA, and IVB iron meteorites, *Science* 271 (1996) 1099–1102.